Supporting information for

Conformational transition of membrane-associated terminally-acylated HIV-1 Nef

Bulent Akgun,[1,2,3] Sushil Satija,[1] Hirsh Nanda,[1,2] Gregory F. Pirrone, [4] Xiaomeng Shi,[4] John R. Engen,[4] Michael S. Kent[5]*

[1]National Institute of Standards and Technology, Gaithersburg, MD
[2]Dept. of Materials Science&Engineering, University of Maryland, College Park, MD
[3]Department of Chemistry, Bogazici University, Bebek 34342, Istanbul, Turkey
[4]Northeastern University, Boston, MA
[5]Sandia National Laboratories, Albuquerque, NM

Supplemental Data

NR measurements for nonmyristoylated dNef adsorbed to monolayers of dDPPG at 30 mN/m.

Fig S1 shows NR data for a monolayer of dDPPG at 30 mN/m on Tris–buffered H_2O subphase along with a scan collected 9 h after injecting 6xHis-dNef at 1 μM. The 6xHis-dNef construct was described previously (Kent, et al 2010). The results show that in absence of N-terminal myristoylation, adsorbed Nef remains in a compact, closed conformation. The fractional coverage was 0.21.

XR measurements: myr-Nef insertion controlled by surface pressure.

Fig 3a and Fig 3b in the main text show XR data for a monolayer of dDPPG at 20 mN/m on Tris–buffered H_2O subphase compared with scans collected after injecting 0.83 μM myr-Nef. The dDPPG monolayer was initially spread to a pressure of ~10 mN/m and then compressed to 20 mN/m. The relatively low final surface pressure facilitated insertion of residues into the lipid monolayer. Insertion was clearly evidenced by a large expansion of the area upon injecting myr-Nef (43% after 6 h at which point the barrier reached the back of the trough). Scans were initiated 2 h, 4 h, and 16 h after injecting myr-Nef, respectively. The XR curve varied with time as adsorption proceeded, the first minimum shifting slightly from 0.06 $Å^{-1}$ to 0.05 $Å^{-1}$ between the first and third scans and the amplitude of the oscillation increasing as well. These changes reflect an increase in the thickness and concentration of the adsorbed protein layer. The peak in the electron density profiles (Fig 3c) at a depth of roughly 20 Å due to the elevated electron density of the lipid headgroups decreased slightly in magnitude upon injecting myr-Nef. The 43% increase in area per lipid molecule accounts for a decrease in the normalized electron density of the headgroups from 1.32 to 1.22 (1+0.32/1.43). That effect is offset somewhat by insertion of residues of the N-terminal arm into the headgroups and displacement of water molecules. For the profile corresponding to the first scan, the portion corresponding to adsorbed Nef is adequately described by a single layer extending 70 Å below the lipid headgroups. The profile of adsorbed Nef corresponding to the third scan contains a maximum displaced 73 Å from the lipid

headgroups. The fractional coverages for the three scans were 0.22, 0.82, and 1.07, respectively. (f > 1.0 can result if the core domains are distributed or staggered over a range of depth relative to the membrane). The coverage for the third scan was higher compared to the coverages for the NR data in Fig 2, Fig 7, and Fig 8 of the main text due to a much longer incubation time.

Fig 4a and Fig 4b in the main text show XR data for a monolayer of dDPPG at 35 mN/m on Tris–buffered H_2O subphase compared with scans collected after injecting 0.83 μM myr-hNef into the subphase. The higher pressure and dense packing of the lipids inhibited insertion of residues into the lipid layer. This was indicated by a lack of change in the area (increase of only 2.5% over 15 h), and absence of a shift in the minimum corresponding to the lipid monolayer thickness, after injecting myr-Nef. The fractional coverages for the two scans in Fig S2 were 0.27 and 0.61. Whereas the profiles in Fig 4c show that the myr-Nef residue density is greatest directly adjacent to the lipid headgroups, there is also a weak extended portion that is not observed in the NR data in Fig 2 or Fig 6. This is most likely a sparse second layer of myr-Nef loosely associated with the primary bound layer. For the run corresponding to the data in Fig 6, 0.5 μM myr-dNef was incubated against the monolayer for 8 hrs and then the concentration was increased to 1 μM for 1 h, at which point adsorption has slowed dramatically and a full scan was collected. This approach appears to have avoided the slight buildup of a second layer. Another possible explanation for the difference is that myr-Nef may be slightly more prone to aggregation than myr-dNef.

Fig S2a and Fig S2b show XR data for a dDPPG monolayer at 25 mN/m on buffer compared with a scan collected 14 h after injecting 0.83 μM myr-Nef and also a scan collected after subphase exchange. The lower final surface pressure (compared to the runs corresponding to the data in Fig 2 and Fig 4) again facilitated insertion of residues into the lipid tail region. During the insertion of myr groups the area increased substantially as was observed at 20 mN/m. The electron density profiles in Fig S2c show that the headgroup density decreased in magnitude upon injecting myr-Nef, indicating insertion into the headgroup layer. The electron density profile at 14 h after injecting myr-Nef shows that myr-Nef is in an extended conformation and contains a maximum displaced 66 Å from the lipid headgroups. After subphase exchange the maximum shifts 10 Å further from the lipid headgroups. This suggests that during subphase exchange electrostatically adsorbed myrNef in closed form was removed and only inserted myr-Nef in open form remained on the membrane. The fractional coverages before and after subphase exchange were 1.11 and 0.80, respectively.

XR measurement of myr-Nef adsorbed to a 70/30 dDPPC/dDPPG monolayer at 20 mN/m

Fig 5a and Fig 5b in the main text show XR data for a 70/30 dDPPC/dDPPG monolayer at 20 mN/m on buffer compared with the third scan collected 22 h after injecting 0.87 μM myr-Nef and a scan collected after exchanging the subphase with buffer. Little difference is observed in the latter two scans. The area expanded 45% after injecting myr-Nef at which point the barrier reached the back of the trough.

The electron density profile (Fig 5c) shows that myr-Nef is in an extended conformation with the core domain displaced ~ 70 Å from the lipid headgroups. The fractional coverage was 0.84.

Fit to the data of Fig 7a in the main text using an ensemble of three Nef structures in which the core domain distance from the membrane was adjusted +/- 10 Å relative to that of the best-fit single structure.

This figure is identical to Fig 7 in the main text except that the fit with an ensemble of three Nef structures involves the best fit single structure combined with structures in which the core domain is displaced 10 Å closer and 10 Å further from residue 22 (weighting of 1:2:1). While providing a better fit than obtained with a single Nef structure, the fit for this ensemble is not nearly as good as for the ensemble in Fig 7b of the main text involving structures with the core domain displaced +/- 20 A from that of the best fit single structure. The best-fit curve shown for the ensemble in Fig S3a (tan line) contains greater oscillations at higher q_z values than are present in the data and the SLD profile contains a maximum that is considerably narrower than that of the profile from the free-form fit.

Figure Captions

Figure S1, related to Figure 2. (a) NR data for a dDPPG monolayer at 30 mN/m on Tris–buffered H_2O subphase (black) along with a scan collected 9 h after injecting 6xHis-dNef at 1 μM (red). b) Best-fit profile band corresponding to the data in a). c) Normalized trough area versus time showing little change of the area upon injection of 6xHis-dNef.

Figure S2, related to Figure 3. (a) XR data for a dDPPG monolayer at 25 mN/m (black) compared with scans collected 12 h after injecting 0.83 μM myr-Nef (cyan) and after subphase exchange with buffer (red). (b) Expanded view of the XR data in a) showing the low q_z region. (c) Electron density profiles corresponding to XR data in a).

Figure S3, related to Figure 7. (a) NR data for a dDPPG monolayer at 20 mN/m on Tris–buffered H_2O subphase (black) and with bound myr-dNef adsorbed from solution at 0.28 μM (red). Best fits are shown using a free-form slab model (red), using a model of Nef with residues 2-22 located in the membrane (blue), and using an ensemble of three Nef structures for which the core domain distance from the membrane was adjusted +/- 10 Å relative to that of the best-fit structure shown in b) (yellow). (b) SLD profiles corresponding to the best-fits in (a).

a)

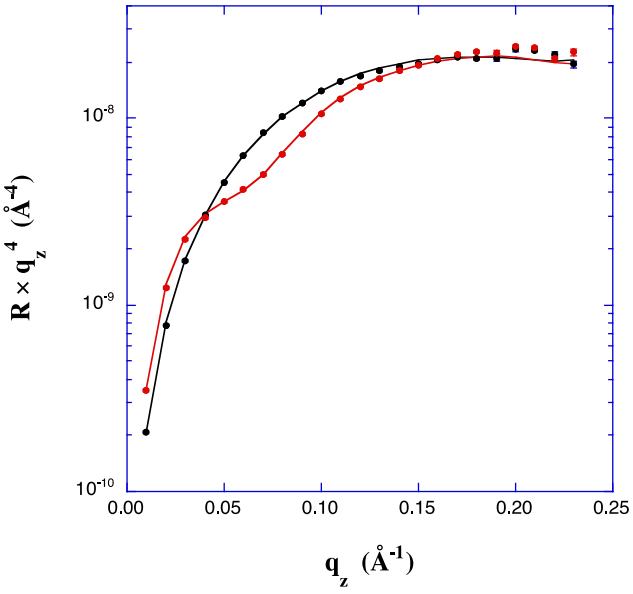

b)

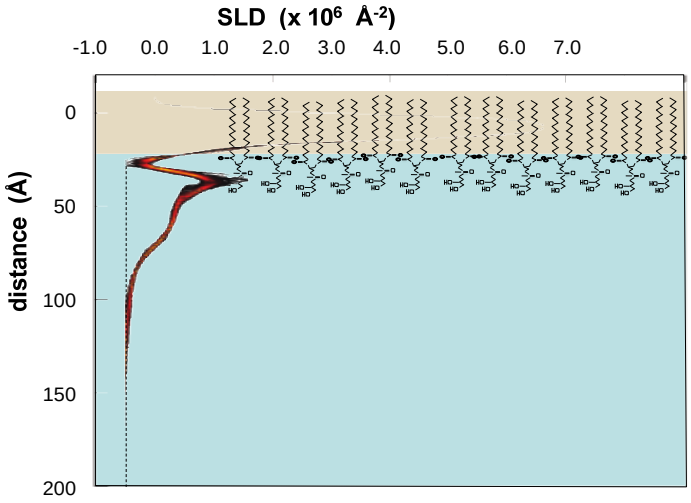

c)

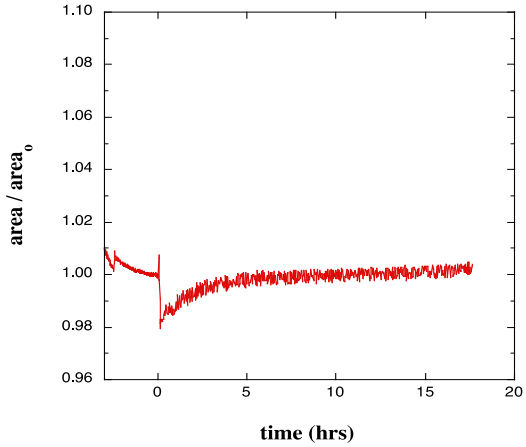

Figure S1.

a)

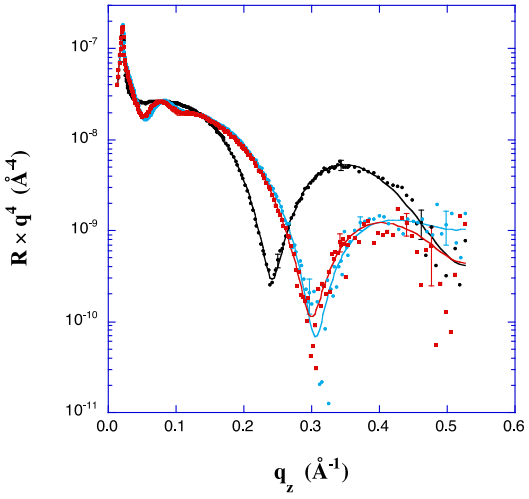

b)

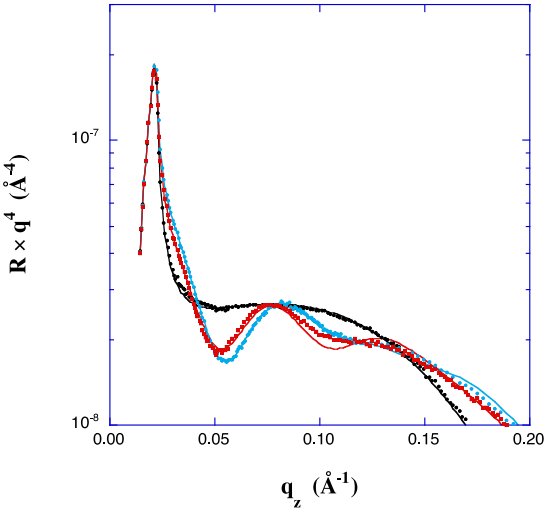

c)

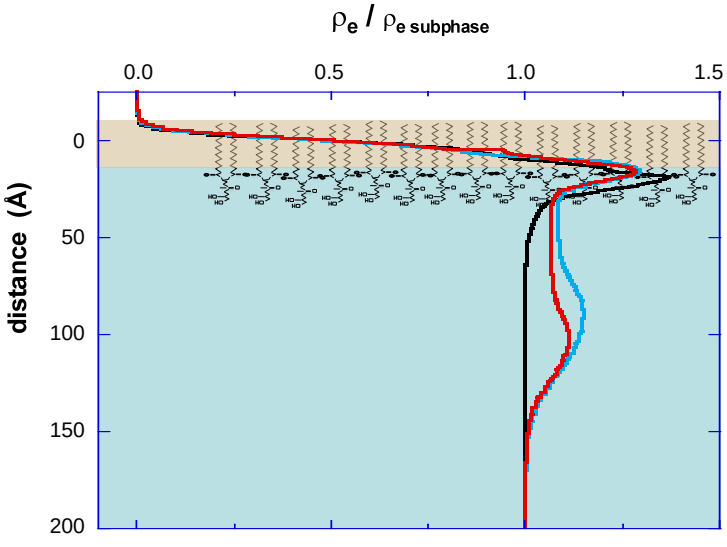

Figure S2.

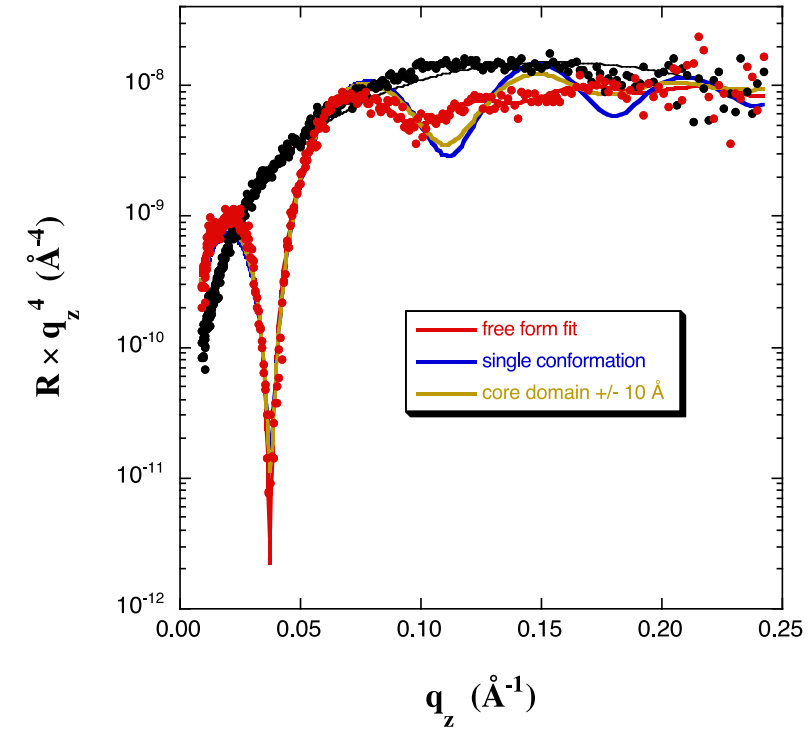
10^{-8}
10^{-9}
10^{-10}
10^{-11}
10^{-12}
$R \times q_z^4$ (Å^{-4})
0.00
0.05
0.10
0.15
0.20
0.25
q_z (Å^{-1})
free form fit
single conformation
core domain +/- 10 Å

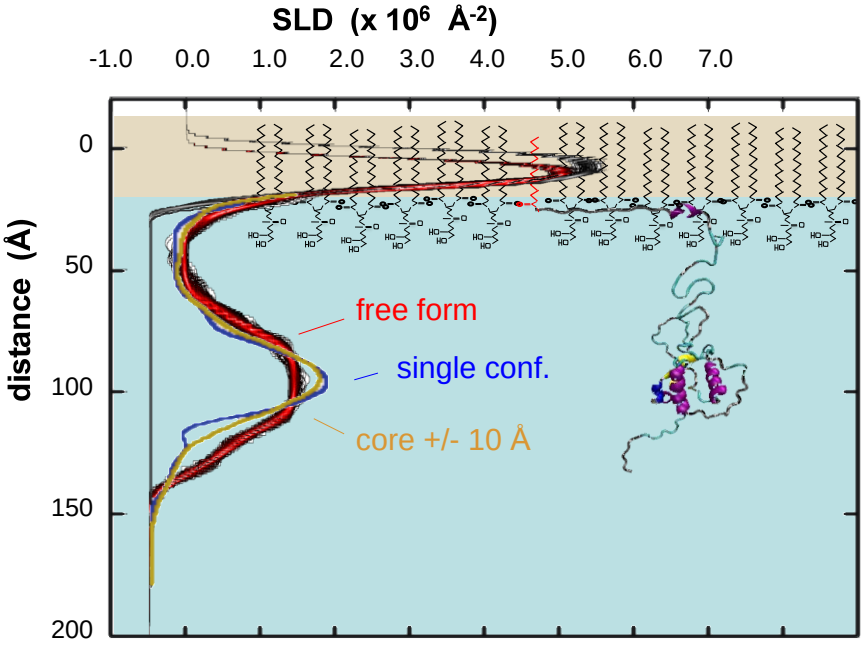
SLD (x 10^6 Å^{-2})
-1.0
0.0
1.0
2.0
3.0
4.0
5.0
6.0
7.0
distance (Å)
0
50
100
150
200
free form
single conf.
core +/- 10 Å

Figure S3.

Supplemental Experimental Procedures

Protocol for NR measurements

Neutron reflectivity (NR) measurements were performed on the NG7 horizontal reflectometer at the National Institute of Standards and Technology (NIST) Center for Neutron Research (NCNR) (Figures 2, 6, 8, and S1) and the Liquids Reflectometer at the Spallation Neutron Source, Oak Ridge National Laboratory (Figure 7). Due to fundamental differences in design for these two spectrometers, the density of sampled data points differed. The measurements on NG7 were performed using a wavelength of 0.475 nm and varying angles of incidence. To maximize the intensity, the sizes of the collimating slits and detector slits were increased during the reflectivity scan and this provided an approximately constant relative q resolution $\Delta q/q$ of 0.04, where $q = 4\pi\sin(\theta)/\lambda$, and θ is the incident and final angle with respect to the surface of the film. All the measurements were done using a 1D PSD detector that ensures the collection of specular and off-specular scattering simultaneously. To obtain the absolute reflectivity, background scattering was subtracted from the specular scattering and the background-subtracted reflected intensity was normalized against main beam. Fig 8 of the main text reports successive scans collected during the adsorption process. These scans were collected over a limited q_z range such that only 1 hr was required to collect each scan. While this collection time is small compared to the timescale of adsorption (4 hr), a small distortion of the curve is inevitable as the data points are collected successively while the adsorbed layer is

changing. However, on the NG7 spectrometer the majority of the collection time for each scan is taken for the last few data points, and so the distortion is mainly present in only those data points and the location of the minimum at $q_z \sim 0.04$ Å^{-1}, that indicates the open form of the protein, is uneffected.

The measurements on the Liquids Reflectometer were performed using a band of wavelengths from roughly 0.375 to 1.06 nm at 14 angles of incidence. The slits were adjusted at each angle to maintain a constant beam footprint on the sample. To obtain the absolute reflectivity, a reflectivity scan was collected with D_2O in the trough. The incident and reflected intensities were also measured at one angle below the critical edge to determine the fraction of total reflected intensity collected at the detector. These data were then used to determine the absolute normalization factor. Reflectivity scans with H_2O buffer were collected using the same slit settings as for the measurements with D_2O. The background subtracted reflectivity was then normalized using the factor determined from the D_2O measurement. With this normalization procedure, NR data for a monolayer of dDPPG on buffer was within 5% of that measured on NG7 for the same conditions.

The average SLDs (neutron and X-ray) for Nef were calculated from the atomic composition and the molecular volume. The molecular volume of Nef was determined using a standard table of amino acid volumes (Stephen J. Perkins, X-ray and Neutron Solution Scattering, New Comprehensive Biochemistry 1985, 143-265).